Performance Enhancement of a Novel Surface Plasmon Resonance Biosensor Using Thallium Bromide

Vasimalla Yesudasu, *Member, IEEE*, and Himansu Shekhar Pradhan, *Member, IEEE*

***Abstract*— In this paper, we present the performance enhancement of the SPR biosensor using a novel dielectric material of thallium bromide (TlBr). The proposed structure comprised of six layers, including BK7 prism, silver (Ag), aluminum arsenide (AlAs), TlBr, black phosphorus (BP), and a sensing layer. In this investigation, we have considered four structures using the above-defined layers for the performance comparison and heightened the impact of TlBr in the proposed SPR sensor. The performance analysis is studied numerically at 633nm wavelength by considering the angular interrogation method and it endorsed with the wavelength variation method as well as the electric field intensity performance, employing the transfer matrix method and the FDTD solutions. The proposed structure is referred to as structure-IV is achieved the sensitivity of 475°/RIU compared to structures- III, II, I that have the sensitivities of 155, 120, 105°/RIU, respectively, at the minimal unit changes in the refractive index of the biomolecules. In addition, the proposed structure facilitates a quality factor of 80.37 and a figure of merit of 79.72. This investigation is introduced the performance of combined sensitive factor (CSF) of 77.9, which shows the SPR's overall performance. In order to observe the wavelength resolution, the sensor's sensitivity is investigated for different wavelengths at different metal thicknesses. Finally, the proposed structure's performance is compared with the existing works, demonstrating that the proposed SPR sensor can be established as a new platform for researchers in the field of bio-sensing applications.**

***Index Terms*— Biosensor, Kretschmann, surface plasmon resonance, thallium bromide, sensitivity.**

I. Introduction

FOR a few decades, many researchers have been increasingly working towards efficient biosensor performance to save human lives against microbial diseases [1]. The primary research area of efficient sensor developers is susceptible and label-free platform devices for bio-molecular detection (ssDNA, blood hemoglobin level and glucose level in urine) and microorganisms in real-time [2]. The Surface Plasmon Resonance (SPR) is a promising label-free device that can detect bio-molecules in real-time with accurate outcomes. Also, it can easily observe the minute variations in the refractive index (RI) of the sensing medium [3]. The SPR sensors are categorized into different types such as prism coupled, fiber optic, grating coupled, and waveguide coupled SPR sensors, based on the light coupling mechanism,. The prism-based SPR sensor favors cautious realization, while the other sensors suffer from the excellent light launching into the fiber core [4]. To simulate the guided or leaky waves, the SPR sensor is considered into two configurations named the Kretschmann configuration (metal film coated over the prism's surface) and the Otto configuration (having an air gap between the prism and metal (P-M) interface) [5]. Many other researchers prefer the Kretschmann configuration due to efficient light coupling from prism to metal film [6]. The P-polarized light applies to the prism as an incident light to excite the surface plasmons (SPs) at the prism-metal (P-M) interface [7]. The electromagnetic wave propagates along with the interfacing a surface plasmon polariton/wave (SPP/SPW) at the metal-dielectric (M-D) interface, and it dies off exponentially to the length of the interface [8]. The SPR geometry is based on the phase matching condition of evanescent wave horizontal component (k_{ev}) with the SPW vector (k_{sp}), i.e., $k_{ev} = k_0\sqrt{\varepsilon_p}\sin\theta_{res} = k_{sp}$ (where, $k_0 = w/c$ represents the incident wave vector, w is the angular frequency, c is the light speed, ε_p is the prism permittivity, and θ_{res} is resonance angle). The SPR resonance condition results in a fall in the reflected wave intensity is determined as the minimum reflectance ($R_{\min}$) due to the total energy of P-polarized incident light transfer to the SPs. The SPR response is obtained by computing the reflectance with an angle through the detector [9]. This response identifies the resonance dip position that can differ due to changes in the sensing medium's refractive index (RI). The amount of RI changes can compute by using the attenuated total internal reflectance (ATR) method. For adequate the SPR biosensor, it requires the exceptional performance of sensitivity (S), quality factor (QF), and figure of merit (FOM) [10]. The SPR's S is directly proportional to the resonance shift, where the QF and FOM judge by the broadness in the reflectance response.

The authors have demonstrated the angular interrogation method to analyze the SPR sensor performance with precious S, QF, FOM measurements [11]. Gold (Au), silver (Ag), copper (Cu) are generally utilized metal films for the SPR

Manuscript received July 29, 2021; accepted September 17, 2021. Date of publication September 21, 2021; date of current version April 1, 2022. *(Corresponding author: Himansu Shekhar Pradhan.)*

The authors are with the Department of Electronics and Communication Engineering, National Institute of Technology Warangal, Warangal, Telangana 506004, India (e-mail: hsp@nitw.ac.in).

Digital Object Identifier 10.1109/TNB.2021.3114225

biosensor design. However, Ag exhibits a high SPR ratio (the ratio between the absolute values of the real and imaginary parts of the dielectric constant), confirming a higher S than other metal films due to poor adsorb biomolecules [12], [13]. The researchers are serving to enhance the SPR performance due to the inadequate traditional sensor of SPR's performance. Many other researchers have been proposed several SPR biosensors based on the nano-particles, nano-holes, metallic nano-slits, and metamaterial for the sensor enhancement [6], [14]–[16]. However, the fastidious control over the SPR geometry and nanostructures' optical features are challenging [17]. Several two-dimensional (2D) materials including graphene, Molybdenum disulfide (MoS_2), and black phosphorus (BP), are used to overcome those challenges because of its higher biomolecular adsorption that leads to the more excellent SPR performance [18], [19]. The authors in [3] reported the influence of BP in the S enhancement of the SPR sensor with the graphene combination. They have used the BP layers to enhance the S, while the graphene monolayer was deposited for higher adsorption biomolecules. The BP improved the S of the SPR sensor as an outgrowth of exceptional mechanical and optoelectrical properties [20], [21]. The extensive performance of the BP-based SPR was proposed in [22]. S. Pal *et al.* reported the S enhancement of SPR employing silicon-BP structure with transition metal dichalcogenides (TDMCs) materials like tungsten disulfide (WS_2) and tungsten diselenide (WSe_2) [23]. Moreover, he proposed the hybrid graphene-BP structure for DNA detection [24]. W. Wu *et al.* proposed the BP-graphene-TDMC structure to enhance the SPR's S, and results found that this structure furnished S, which is 2.4 times higher than the traditional SPR sensor [25]. A. Srivastava *et al.* also proposed several structures for SPR performance enhancement using BP alloy structures [26], [27]. The BP adsorption energy is higher than the graphene and MoS_2; the response was 40 times faster than all other 2D materials due to the billion-level sensing ability of analyte and puckered lattice configuration [2]. Y. Cai *et al.* was demonstrated that electric characteristics, including bandgap, working function, and carrier effective mass, are inversely proportional to the number of BP layers. Hence, BP can be suitable for efficient biomolecule binding [28]. The high RI of a dielectric layer is coated over a plasmonic material, leading to enhance the field intensity in the sensing layer of the sensor [3]. N. Mudgal *et al.* presented the performance enhancement of graphene-affinity layer-based SPR sensor for bacterial detection employing the $BaTiO_3$ material as a dielectric layer. This sensor performance was analyzed numerically at visible wavelength and obtained the maximum performance in terms of S, QF, and detection accuracy (DA) [29]. L. Liu proposed the graphene-$BaTiO_3$-based and ZnO-based SPR sensor for S enhancement using the Ag-Au structure [30], [31]. Furthermore, aluminum arsenide (AlAs) is a dielectric material, enhancing the SPR sensor's performance due to the high RI value. In 1969, D. J. Stukul stated the energy band structure of the AlAs clusters [32]. H. T. Minder introduced its optical properties in 1970, and L. Guo described the design, electric and energetic features in 2011 [33], [34]. In addition, this paper presents the novel bromide dielectric material, i.e., thallium bromide (TIBr), to improve the SPR's performance in terms of S, QF, FOM, and combine sensitivity factor (CSF). The TlBr is a dielectric material with vast bandgap energy, a compound semiconductor with high gamma-ray stopping power and promising physical properties. Also, the TIBr performance minimizes the polarization effect. Thus, the proposed structure comprised of BK7 prism, Ag, AlAs, TIBr, BP, and sensing medium to analyze the biosensor performance. The organization of the present paper is as follows. Section-2 explains the theoretical and numerical modelling of the proposed SPR biosensor. The result and discussion for the proposed design are reported in section-3. Moreover, section-4 describes the proposed design and its field distributions using Finite-difference time-domain (FDTD) solutions. Finally, section-5 concludes the present work.

II. Theoretical and Numerical Modelling of the Proposed SPR Biosensor

This section explains the theoretical and numerical modelling of the proposed SPR sensor, which includes the SPR design consideration and its performance parameters.

A. Theoretical Modelling

The transfer matrix method has been used for N-layer modelling to compute the proposed sensor's reflectivity (R_p) due to its efficiency as well as not required any approximations. Let assume that the k^{th} layer's thickness of d_k is considered along the Z-axis, ε_k signifies the dielectric constant of k^{th} layer. By employing the boundary conditions, the tangential field at $Z = Z_1 = 0z = z_1 = 0$ are presented regarding of tangential field at $z = z_{N-1}$ as follows in Eq. (1):

$$\begin{bmatrix} A_1 \\ B_1 \end{bmatrix} = C_{ij} \begin{bmatrix} A_{N-1} \\ B_{N-1} \end{bmatrix} \tag{1}$$

where, A_1 and B_1 symbolizes the tangential components of electrical and magnetic fields, respectively, at the first layer boundary. A_{N-1} and B_{N-1}BN-1 are corresponding fields for the N^{th} layer boundary. The C_{ij} signifies the properties matrix of the SPR sensor combined structure, and for P-polarized incident light, it can be given as Eq. (2).

$$C_{ij} = \left[\prod_{K=2}^{N-1} \begin{pmatrix} \cos\beta_k & -i\sin\beta_k/e_k \\ -ie_k\sin\beta_k & \cos\beta_k \end{pmatrix}\right]_{if} = \begin{bmatrix} C_{11} & C_{12} \\ C_{21} & C_{22} \end{bmatrix} \tag{2}$$

where, Eq. (3) denotes a description of the transverse RI. Moreover, Eq. (4) measures the arbitrary stage constant β_k for the k^{th} layer, whereas Eq. (5) and (6) represent the wave impedance (z_k) and input angle (θ_k) for k^{th} layer. Here, λ are the wavelength of an incident light beam, n_p is the prism's RI, θ is the incident angle, μ_k is the permeability of the k^{th} layer [35].

$$n_k = \left[\frac{\mu_k}{\varepsilon_k}\right]^{1/2} \quad \cos\theta_k = \sqrt{\frac{\varepsilon_k - (n_p\sin\theta)^2}{\varepsilon_k^2}} \tag{3}$$

$$\beta_k = \frac{2\pi}{\lambda} n_k \cos\theta_k (z_k - z_{k-1}) = \frac{2\pi}{\lambda} d_k \sqrt{\varepsilon_k - (n_p \sin\theta)^2} \tag{4}$$

$$z_k = \frac{k_x n_k \cos\theta_k}{(2\pi c/\lambda_{633})\, \varepsilon_k^2} \tag{5}$$

$$\theta_k = \left(\cos\sqrt{1 - (n_{k-1}/n_k)(\sin\theta)^2}\right)^{-1} \tag{6}$$

Finally, Eq. (7) and (8) denote the mathematical expressions of Fresnel's R_p mode analysis for computing the R_p and reflection coefficient (r_p) of an incident light, respectively [35].

$$R_p = |r_p|^2 \tag{7}$$

$$r_p = \frac{(C_{11} + C_{12} n_N)\, q_1 - (C_{21} + C_{22} n_N)}{(C_{11} + C_{12} n_N)\, q_1 + (C_{21} + C_{22} n_N)} \tag{8}$$

The S define as the ratio of change in SPR resonance angle ($\nabla\theta_{SPR}\nabla\theta_{res}$) to change in the RI ($\nabla n$) and is a crucial factor for a better SPR sensor. The sensor's high sensitivity performance with little variation in analyte (biomolecules) concentration demonstrates the sensor's better sensing capabilities, as it can detect extremely minute structural differences. In addition, this study computes performances of QF, FOM, and combined sensitivity factor (CSF), demonstrating the quality of the sensor. The mathematical expressions to compute above-defined parameters are shown in Eq. (9-12), whereas FWHM is the full width half maximum and $R_{\max}$ is the maximum reflectivity in the reflectance curve [22], [36]. The performance of the quality factor and figure of merit report the product quality, noise impact in a sensor, respectively. Finally, the sensor's overall performance is investigated with the combined sensitivity factor.

$$S = \frac{\nabla\theta_{res}}{\nabla n} \tag{9}$$

$$QF = \frac{S}{FWHM} \tag{10}$$

$$FOM = S\frac{(1 - R_{\min})}{FWHM} \tag{11}$$

$$CSF = S \times \frac{R_{\max} - R_{\min}}{FWHM} \tag{12}$$

B. Numerical Modelling

The schematic structure of the proposed SPR sensor for bio-sensing applications (i.e., ssDNA) has presented in Fig. 1. The Kretschmann SPR biosensor consists of six layers, and all layers' RI are operated at 633nm wavelength. For this structure design, we utilize the BK7 prism as the first layer (n1) to offers the minimum Kerr factor, having the RI of 1.515 [23]. The second layer (n2) is encompassed of Ag, as coated over the prism base with a complex RI of 0.056266+4.27761i. In addition, the dielectric layers, such as AlAs and TIBr, are deposited on Ag for protection against oxidation and enhanced sensor performance. The third and fourth are comprised of AlAs and TIBr, as coated over the Ag with RI of 3.1099 and 2.5728, respectively. The Ag and TIBr's thickness is optimized by applying the iteration method, where the constant thickness of AlAs is 5nm. The fifth layer (n5) is BP deposited over the TIBr with an RI of 3.5+0.01i and a thickness of 0.53nm [23]. Finally, the sixth layer (n6) is a sensing medium for the water biomolecules adsorption, and RI varies from 1.33 to 1.332. This proposed structure observes the performance for minute variation in the adsorption molecules. To compare the proposed structure's performance, we have considered three other dissimilar SPR structures with the above-defined layers.

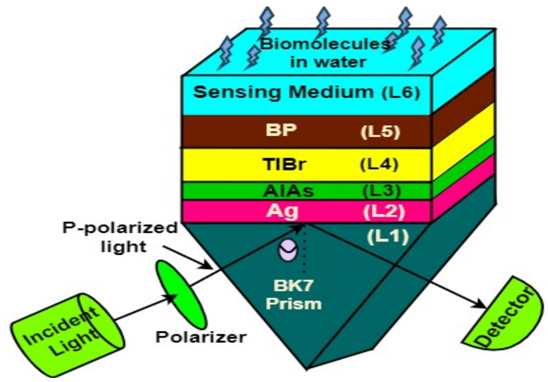

Fig. 1. Proposed SPR biosensor structure ("L" denotes the Layer).

III. Results and Discussion

A. Ag and TIBr Thickness Optimization

The proposed SPR sensor requires the optimized thickness of Ag and TIBr for analyzing the optimized performance. This thickness optimization is obtained from the performance of $R_{\min}$ by the applying iteration process. The reason for it is that many other researchers were optimized their proposed SPR structures by applying the iteration method [22], [23], and [29]. V. Yesudasu *et al.*, 2020 and N.Mudgal *et al.*, have optimized their layer structures from the $R_{\min}$ performance. Fig. 2(a-c) presents the reflectance responses for different thicknesses of Ag (i.e., 40-50nm with an interval of 5nm) and TIBr (i.e., 1-7nm with an interval of 2nm), whereas the residual layers have constant thicknesses, i.e., AlAs of 5nm, and BP of 0.53nm. Fig. 2(a) shows the reflectance responses in terms of an angle for the different TIBr thicknesses, whereas Ag is remained at 40nm thickness. The obtained results are $R_{\min}$ of 0.3418, 0.3071, 0.1720, and 0.7808 at resonances angles of 75.05, 78.35, 83.52, and 86.38° for assigned TIBr thicknesses, respectively. The variations in $R_{\min}$ is occurred due to the spatial extension of SPs in a medium that depends on SP's propagation length (PL) in the parallel direction. The PL is a distance in propagation direction covered by SPs, decaying exponentially due to losses within the metal by the electron factor [3].

Similarly, Fig. 2(b) displays the reflectance responses at a constant thickness of Ag is 45nm. The attained $R_{\min}$ of 0.1657, 0.1277, 0.0081, and 0.9023 at resonance angles of 75.22, 78.79, 84.85, and 85.46° for allotted TIBr thicknesses, respectively. Finally, Fig. 2(c) represents the reflectance responses at a constant thickness of Ag is 50nm. The acquired $R_{\min}$ of 0.0383, 0.0166, and 0.0803 at resonance angles of 75.32, 79.13 and 86.01° for the TIBr thicknesses of 1nm, 3nm, and

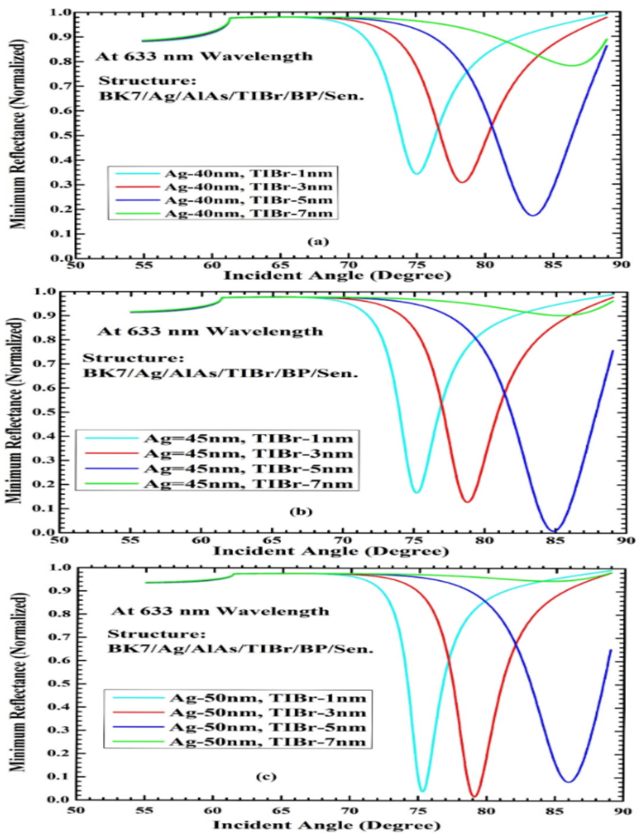

Fig. 2. Ag and TIBr Optimization by employing angular interrogation method. Reflectance responses for different TIBr thickness (a) at constant of Ag thickness of 40nm (b) at constant of Ag thickness of 45nm (c) at constant of Ag thickness of 50nm.

5nm, respectively. At thickness of 7nm, the resonance dip is distressed by the limitation resonance condition (i.e., the total energy of SPs transfer to the detector) and loss of the metal electron factor. The outlined measurements of $R_{\min}$ and resonance angles for fig. (a-c) are represented in Table I, which is demonstrated that less $R_{\min}$ is generated at the Ag and TIBr thickness of 45nm and 5nm, respectively. Hence, the authors have concluded the optimized thickness values of Ag and TIBr are utilizing in the proposed SPR sensor for further performance analysis. After optimizing layers thicknesses, the parameter list and different structures for the proposed work has been presented in Table II and III successively, which are utilized for further investigation of this study.

B. Proposed SPR Performance Comparison

The reflectance curve of the proposed structure-4 is compared with the other structures (1, 2, and 3), as shown in Fig. 3. In the comparison process, we have considered the RIs, before and after adsorption as 1.33 and 1.332, indicating the RI's minute variation for computing the performance parameters in terms of S, QF, FOM, and CSF. The solid and dotted SPR reflectance curves signify before and after adsorption, and cyan, blue, red, and green colors are indicated for structures-I, II, III, and IV, respectively. The outlined performance measurements of Fig. 3 have been mentioned in Table IV, which can

TABLE I
PARAMETERS LIST FOR DESIGNING THE PROPOSED SPR STRUCTURE

Ag Thickness	TIBr Thickness	Refractive Index (RI)	Thickness
40	1	0.3418	75.05
40	3	0.3071	78.35
40	5	0.1720	83.52
40	7	0.7808	86.38
45	1	0.1657	75.22
45	3	0.1277	78.79
45	5	0.0081	84.85
45	7	0.9023	85.46
50	1	0.0383	75.32
50	3	0.0166	79.13
50	5	0.0803	86.01
50	7	-	-

TABLE II
THE LIST OF DESIGNED PARAMETERS OF PROPOSED STRUCTURE OF SPR BIOSENSOR

Layer	Refractive Index (RI)	Thickness
BK7-prism	1.515	-
Silver (Ag)	0.056266+4.27761i	45nm
Aluminum arsenide (AlAs)	3.1099	5nm
Thallium Bromide (TIBr)	2.5728	5nm
Black Phosphorus (BP)	3.5+0.01i	0.53nm
Sensing medium	1.33-1.332	-

TABLE III
THE LIST OF CONSIDERED SPR STRUCTURES FOR PROPOSED WORK

Structure No.	SPR Biosensor Name	Combination
I	Conv.	BK7-Ag- Sen.
II	BP-based	BK7-Ag- BP-Sen.
III	AlAs-based	BK7-Ag-AlAs-BP-Sen.
IV	Proposed	BK7-Ag-AlAs-TIBr-BP-Sen.

demonstrate that FWHM and change in resonance angle are increased from structure-I to IV. The SPR parameters of S, QF, FOM, and CSF are measured using Eq. (7-10). The SPR sensor has a maximum S of 105deg/RIU for structure-I, 120°/RIU for structure-II, 155°/RIU for structure-III, and 475°/RIU for structure-IV. The S of the structure-II (i.e., BP-based SPR) is greater than the structure-I (i.e., conventional SPR) due to its exceptional properties, including the low dielectric losses, the high RI, the high molar mass of the substance (233.192 g/mol), crystal forms of a perovskite structure, and high-density value (6.02 g/cm^{-3}) [18].

Similarly, structure-III (i.e., AlAs-based SPR) has furnished more S than structure-II because of the high work function of a bandgap of 2.16 eV, a high dielectric constant of 10.9, and a high-density function of 3.81 g/cm3. Also, its cubic crystal structure offers more efficient biomolecules bindings on the AlAs surface [37]. Finally, structure-IV (i.e., proposed SPR) is accomplished the noteworthy S, which is a huge

TABLE IV
COMPARISON OF MEASURING SPR PERFORMANCE PARAMETERS SUCH AS S, QF, FIGURE OF MERIT (FOM) AND COMBINE SENSITIVITY FACTOR (CSF) OF PROPOSED STRUCTURE WITH THE OTHER THREE STRUCTURE

SPR Biosensor	Resonance angle (°)		Performance Parameters					
	1.33	1.332	$\nabla\theta_{res}$	FWHM	S (°/RIU)	QF (RUI^{-1})	FOM	CSF
I. Conv.	67.52	67.73	0.21	1.09	105	96.33	78.31	77.91
II. BP-based	67.97	68.21	0.24	1.18	120	101.69	82.90	82.47
III. AlAs-based	73.82	74.13	0.31	2.42	155	64.05	52.90	52.70
IV. Proposed	84.85	85.80	0.95	5.91	475	80.37	79.72	77.90

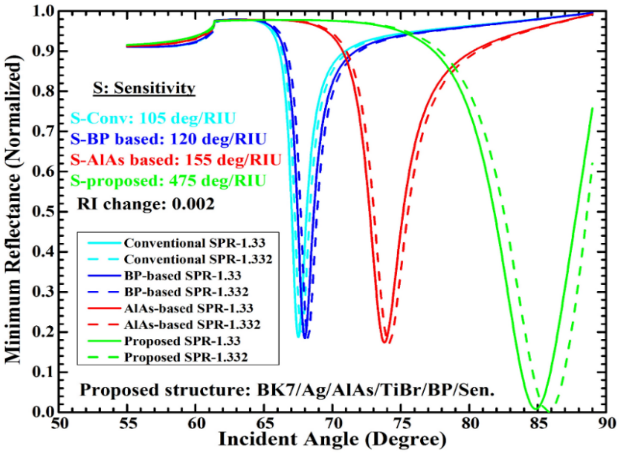

Fig. 3. Reflectance responses vs an angle for all defined structures, such as Conventional (S1: BK7/Ag/Sen.), BP-based (S2: BK7/Ag/BP/Sen.), AlAs-based (S3: BK7/Ag/AlAs/BP/Sen.), Proposed (S3: BK7/Ag/AlAs/TIBr/BP/Sen.) SPR biosensor.

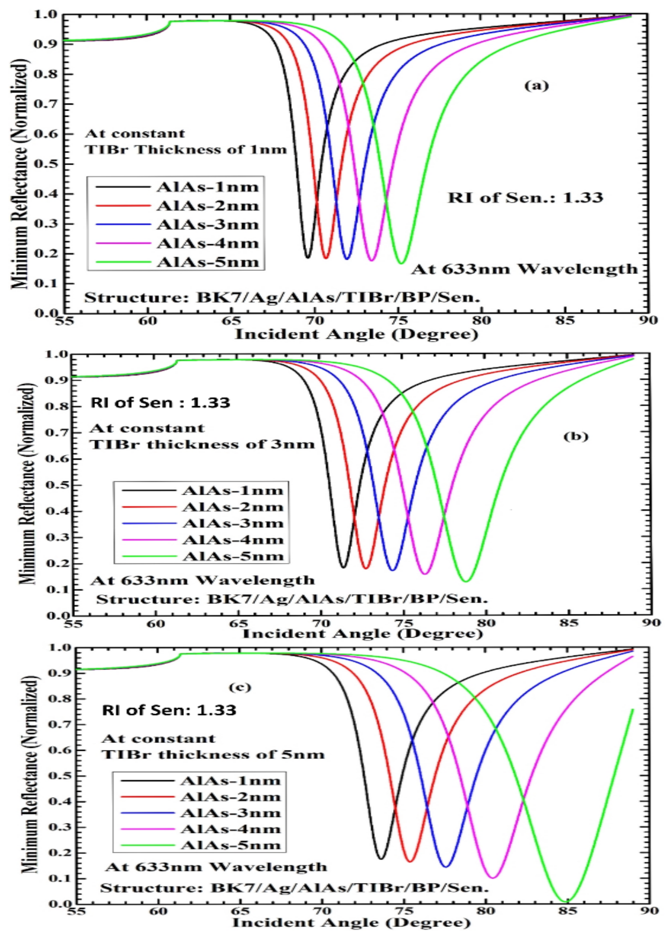

Fig. 4. Reflectance responses vs an angle for different AlAs thicknesses (a) at constant TIBr thickness of 1nm (b) at constant TIBr thickness of 3nm (c) at constant TIBr thickness of 5nm.

performance enhancement than the structure-III. The reasons behind this enhancement are the high RI value, the high bandgap of 2.68 eV, the high thermal expansion coefficient of 51×10^{-6}/°C, the vast density factor, and the dielectric constant of 7.50 g/cm3 and 30.3, successively [37]. However, after adding the TIBr bromide material, the SPR sensor offers massive S but increased broader SPR response, i.e., FWHM due to damping [39]. In addition, the proposed sensor is presented the acceptable QF, FOM, and CSF even though it has high FWHM. The furnished QF of 80.37, FOM of 79.72, and 77.90 for the proposed SPR sensor, i.e., structure-IV. This study mainly focus on the sensitivity performance of SPR because in the literature study, it has been found that the sensitivity is one of the most important parameters for analyzing a high performance SPR biosensor. Moreover, many researchers have been explored several structures in order to improve the SPR sensitivity performance only. In addition, the higher sensitivity with minute variation in the biomolecules shows the quick response of the sensor, which is one of its great advantages. Therefore, though, structure-II has a little bit higher performance in terms of QF, DA, FOM and CSF, it has a huge difference in terms of sensitivity. Therefore, the TIBr-based SPR, i.e., the proposed structure, is useful to enhance the SPR biosensor for bio-sensing applications (e.g., ssDNA) and open a novel way for TIBr utilization bio-sensing region.

C. Analysing the Impact of TIBr in the Proposed SPR

Moreover, the effect of TIBr in the proposed SPR structure is observed from Fig. 4, which shows the reflectance responses for increasing AlAs layers. The reflectance responses in Fig. (4a) are drawn for different AlAs layers at the TIBr constant thickness of 1nm, and similarly, Fig. (4b) at 3nm and Fig. (4c) at 5nm. Fig. 4 is clearly witnessed that a resonance shift occurred at each layer of AlAs. From Fig. 4(a-c), the performances resonance shift change and $R_{\min}$ are contrary to each other because of the low extinction coefficient of AlAs and TIBr [39]. The FWHM of these SPR responses

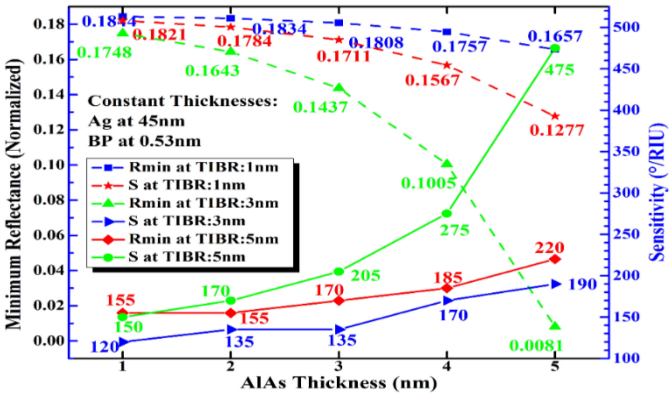

Fig. 5. Graphical representation of R_{min} and S of proposed sensor for different AlAs and TlBr thicknesses at constant thickness of Ag of 45nm, BP of 0.53nm.

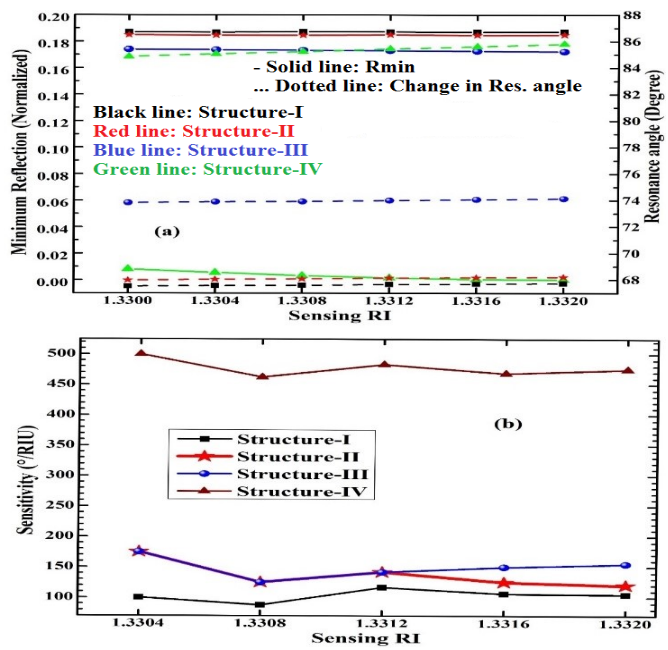

Fig. 6. (a) Graphical representation of R_{min} values and resonance angles with cover sensing RI for structures-I, II, III and IV at λ of 633nm (b) S variation with cover sensing RI for structures-I, II, II I and IV at λ of 633nm.

increases with the number of AlAs and TlBr layers due to SPs damping [39]. Fig. 5 presents the graphical representation of measurement of $R_{\min}$ and S for all responses in Fig. 4; Therefore, the extreme S of 190°/RIU for Fig. (4a), 220°/RIU for Fig. (4b) and 475°/RIU for Fig. (4c), respectively. Fig. 6(a-b) are plotted as the graphical representation of variations in R_{min} $R_{\min}$, resonance angle, and S, respectively concerning the sensing RI. Furthermore, Fig. (6a) explored the structure-IV offer a shallow value of R_{min} than all other structures, i.e., I, II and III. Hence, the structure-IV transfers maximum energy of incident light to the detector, contrary to other structures. The resonance angle is directly proportional to the sensing RI. Fig. (6b) has exhibited the S's variations with respect to the sensing RI. The structure-IV is enhanced a huge S than the structure-III, which is better than structure-II and I.

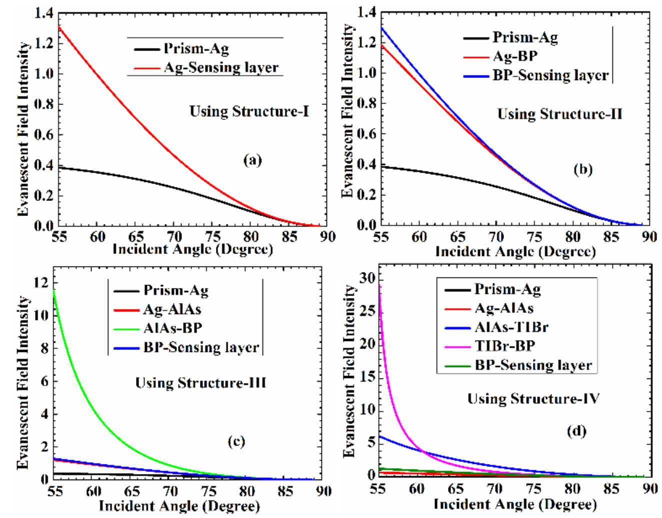

Fig. 7. Measurement of evanescent field intensity of each interface with respect to an incident angle for all structures (a) Structure-I (b) Structure-II (c) Structure-III, and (d) Structure-IV.

D. Performance Measurement of Evanescent and Electric Field Intensity for Proposed SPR Sensor

The evanescent field intensity (EFI) or electric field enhancement factor (EFEF) is a function of both incident light angle and its polarization components. The EFI and EFEF are utilized for the vibrations of p-polarized vectors as a function of the coordinate system at the interface plane, which is defined as being parallel to the exciting light beam. Eq. (13) and (14) are mathematical expressions for computing the EFI and EFEF, respectively [38]. Where, n is the ration of N^{th} layer and prism's RI, t is the transmittance coefficient of the SPR sensor.

$$EFI = \frac{4\cos^2\theta\,\sin^2\theta}{\left(1-n^2\right)\left[\left(1+n^2\right)\left(\sin^2\theta-n^2\right)\right]} \tag{13}$$

$$EFEF = \frac{\varepsilon_1}{\varepsilon_n}\,|t|^2 \tag{14}$$

Fig. 7(a-d) explores the (EFI) at each surface interface for all structures, including I, II, III, and IV. The sensor accomplished the high EFI at the Ag-Sensing interface for structure-I, BP-sensing interface for structure-II, AlAs-BP interface for structure-III, and TlBr-BP interface for structure-IV. The structure-II to IV confirms that the BP of 2D-material increases the field intensities, and the TlBr-BP interface is furnished high-intensity factor rather than all other interfaces. The EFI is decayed to zero at the end of the angular variations. Fig. 8 presents the electric field enhancement factor (EFEF) with respect to an incident angle for all structures, which can be measured by Eq (11) [39]. In the literature, it is well known that the field intensity is inversely proportional to the reflectivity (i.e., its extreme value of field intensity is minimum in the reflectivity). The greater SPs' excitation is transpired at the instant of strongest field intensity due to less R_{min}. From Fig. 8, it easily concluded that the structure-IV generates high EFI, which symbolizes greater SPs excitation, than all other structures, i.e., structure-III, II, and I.

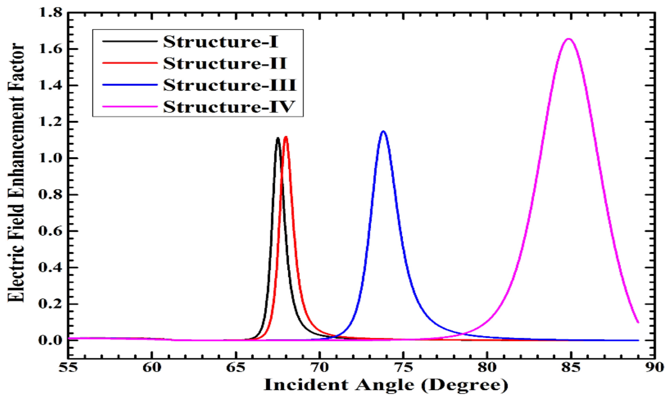

Fig. 8. Representation of electric field enhancement factor vs Incident angle for all structures.

E. Comparative Study of SPR Performance Analysis

Finally, Table V presents a comparative study between the proposed structure's performance and existing structures. The proposed structure furnished the enhanced S of 475, QF of 80.37, and FOM of 79.72. Moreover, it also introduced the novel SPR parameter, i.e., CSF of 77.90. Therefore, the presented comparative study reveals that the proposed SPR sensor furnishes an agreeable solution for bio-sensing applications, such as ssDNA, with high S, QF, FOM, and CSF.

F. Performance Analysis of Proposed SPR Sensor for Different Wavelengths

For a better understanding of the proposed sensor, the performance shows the reflectance intensity with respect angle for different wavelength regions at three metal thicknesses. The RIs for each layer at different wavelengths have been obtained from the equations in [22] and [37]. Fig. 9 depict reflectance responses for different wavelength regions, such as 630, 650, 670, 690, and 700nm at sensing RI of 1.33, whereas Fig. (9a), (9b), and (9c) represent for Ag thickness of 40, 45 and 50nm, respectively. Fig. (10a), (10b), and (10c) explore similar types of responses at the sensing RI of 1.332.

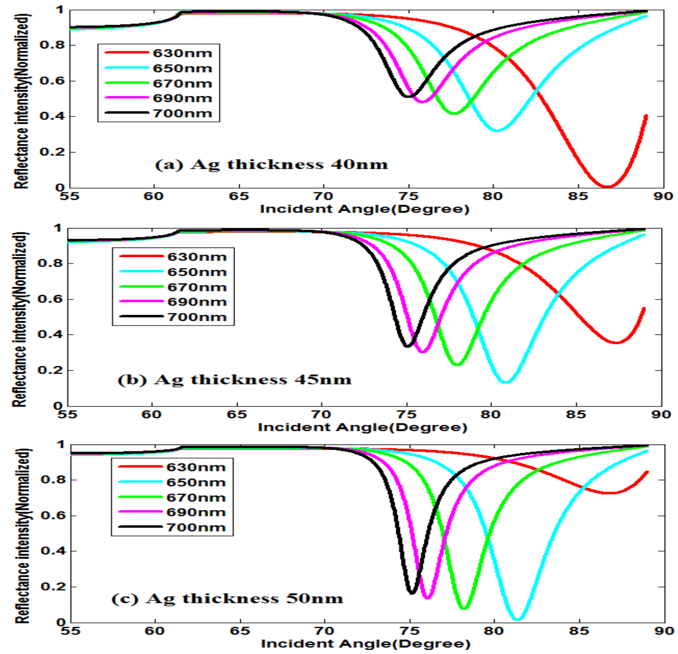

Fig. 9. Reflectance intensity measurement using angular interrogation for different wavelengths at sensing biomolecule RI of 1.33 (a) Ag thickness of 40 nm (b) Ag thickness of 45 nm (c) Ag thickness of 50 nm.

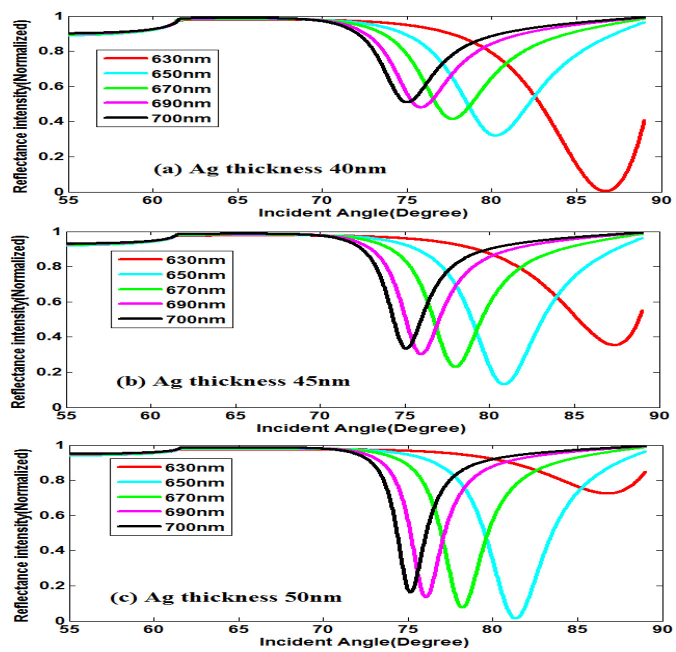

Fig. 10. Reflectance intensity measurement using angular interrogation for different wavelengths at sensing biomolecule RI of 1.332 (a) Ag thickness of 40nm (b) Ag thickness of 45nm (c) Ag thickness of 50nm.

IV. Performance Analysis of Proposed SPR Sensor Using FDTD

The Finite-difference time-domain (FDTD) is a numerical analyzed technique, using for modelling computation electrodynamics. Fig. 12 represents the proposed SPR sensor structure design by considering the Lumerical FDTD solution, whereas, Fig. 12(a) perspective view, Fig. 12(b) xy view, Fig. 12(c) xz view, and Fig. 12(d) yz view. The fabrication process used the structural modelling and also added the respective materials to create a complete structure. The objective editor of FDTD technique sets the RIs and all other parameters as default, where all utilized parameters have considered as generalized measurement parameters including the substrate width of sensor. The design parameters for the proposed SPR using FDTD are shown in Table VI. The design process has considered the perfectly matched layer (PML) boundary conditions around the structure, auto non-uniform mesh with an accuracy of 2 for protection from the mechanical and mechanical defects. The obtained results in terms of change in resonance angle ($\nabla\theta_{res}$) and S are exhibited in Fig. 11. The results demonstrated the highest $\nabla\theta_{res}$ of 0.85 and S of 425°/RIU are achieved for the wavelength region of 630nm at Ag thickness of 40nm. Therefore, it signifies that the proposed structure furnish magnified

TABLE V
COMPARISON STUDY OF PROPOSED SPR STRUCTURE'S PERFORMANCE WITH EXISTING WORK AT VISIBLE WAVELENGTH

COMPARISON STUDY OF PROPOSED SPR STRUCTURE'S PERFORMANCE WITH EXISTING WORK AT VISIBLE WAVELENGTH.

Ref. No	Utilized technique	Structure of the SPR sensor	S *(deg/RIU)*	QF *(RIU^{-1})*	FOM	CSF
[20]	Prism	Prism/Au/BP	180	-	-	-
[41]	Prism	Prism/Air/MoS2/Al/MoS2/graphene	190.83	-	-	-
[42]	Prism	Prism/Au/MoS2/Au/graphene	182	-	-	-
[43]	Prism	Prism/Ag/PtSe2	162	-	14.93	-
[43]	Prism	Prism/Au/PtSe2	165	-	14.12	-
[44]	Prism	Prism/Ag/PtSe2/WS2	194	34.22	17.64	-
[44]	Prism	Prism/Au/PtSe2/WS2	187	29.39	15.72	-
Proposed work	Prism	Prism/Ag/AlAs/TIBr/BP	475	80.37	79.72	77.90

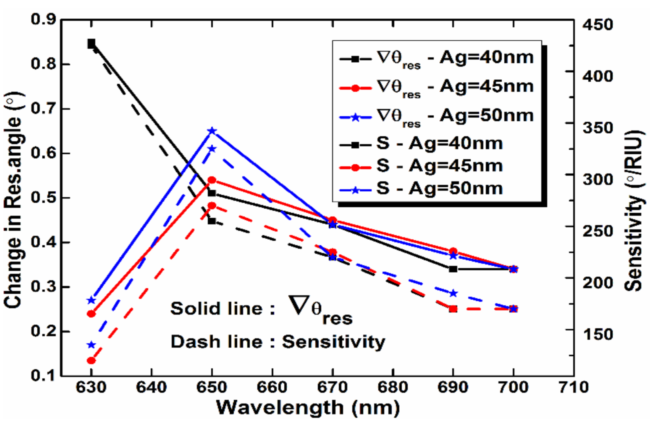

Fig. 11. Measured parameters such as change in resonance angle and S for Fig. 9 and 10.

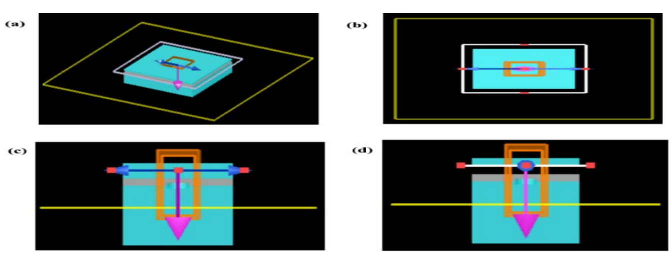

Fig. 12. Proposed SPR sensor design by considering Lumerical FDTD solution (a) Perspective view (b) xy view (c) xz view and (d) yz view.

performance at 630nm wavelength region, which is proved by using the angular variation method as well as the wavelength variation method. The larger wavelength region can applicable for SPR sensor at the larger metal film thicknesses. However, previous research has shown that lower wavelengths offer low penetration depth with traditional SPR, resulting in lower SPR performance, but this research reveals contrary with a SPR structure using a novel dielectric material TIBr. Therefore, an incident optical radiation absorbs into plasmonic modes in the proposed SPR sensor, resulting in standing waves on the metal film. These waves drive strong EM fields that are existing at the prism and metal interface. Furthermore, Fig. 13(a-c) depicts the spatial distribution for the fundamental mode of E-field magnitude (|E|), H-field magnitude (|H|), and power amplitude (|P|), respectively in the proposed SPR sensor. Similarly, Fig. 14(a-c) shows spatial distributions for

TABLE VI
DESIGN PARAMETERS FOR PROPOSED SPR USING FDTD

	Axes boundary (μm)			Additional Parameters
	X-span	Y-span	Z-span	
zBK7	0-20	0-20	-4 – 0	-
Ag	0-20	0-20	0-0.45	-
AlAs	0-20	0-20	0.45-0.95	-
TIBr	0-20	0-20	0.95-1.45	-
BP	0-20	0-20	1.45-1.503	-
Sensing	-	-	1.503-1.523	Radius =2 μm
FDTD	0-6	0-6	0-4	Simulation time= 5000Hz, Stability factor=0.99 and time step=0.0061657.
Source	0-24	0-24	0-1	Z-axis in Backward direction
Transmittance	0-50	0-50	-1.5 - 0	2D Z-normal

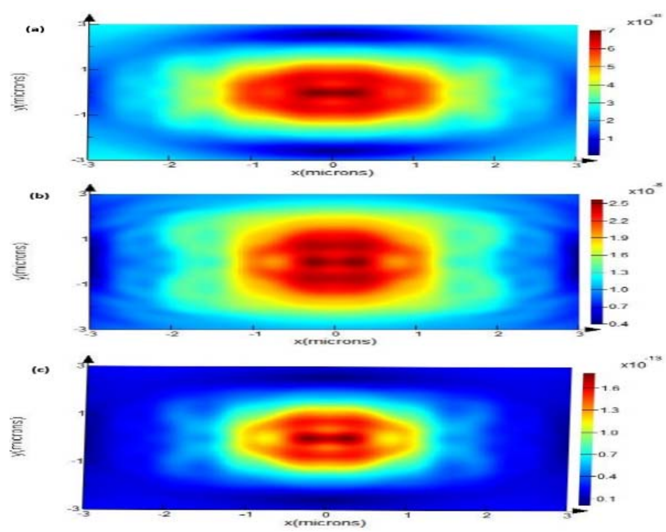

Fig. 13. Enhancement of the field and power distribution of fundamental mode in the proposed SPR structure by employing Yee's technique (a) E-field (b) H-field (c) Power distribution field.

SPP mode of E-field, H-field, and power amplitude, respectively. From the field and power distribution of the proposed SPR sensor, it can be found that at E-field magnitude has more ability to strike the metal surface's free electrons in the fundamental mode and the SPP mode. Finally, the analysis

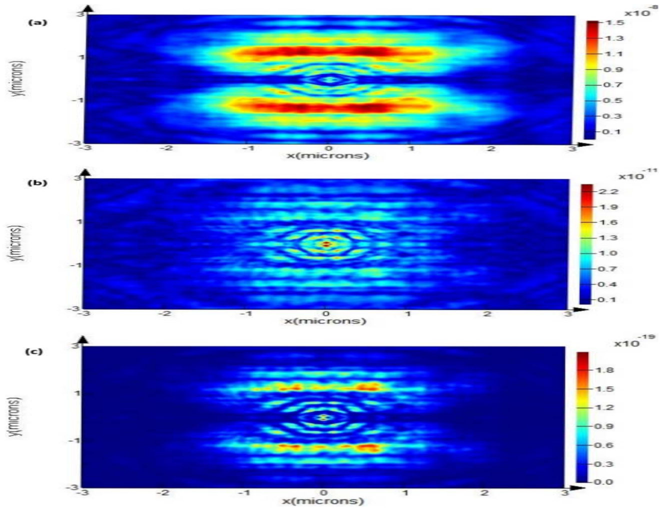

Fig. 14. Enhancement of the field and power distribution of SPP mode in the proposed SPR structure by considering FDTD solution tool (a) E-field (b) H-field (c) Power distribution field.

can demonstrate that the incident light is efficiently coupled into plasmonic modes for Ag metal surface, leading to higher SPR performance.

V. Conclusion

A highly enhanced performance of SPR biosensor has been proposed in this paper at 633nm wavelength using numerical analysis. In addition to the proposed structure, we have considered three other structures for the performance comparison. For optimizing the Ag thickness of 45nm and TIBr thickness of 5nm by iteration method of Fresnel's R_p mode analysis, the SPR reflectance responses are plotted and accomplished a low R_{min} and high resonance shift. Further, the performance analysis has done for all structures and found the maximum S is 475°/RIU for structure-IV, 155°/RIU for structure-III, 120°/RIU for structure-II, and 105°/RIU for structure-I. It is clearly observed from the results that the S of the structure-IV is 4.52, 3.96, 3.06 times higher than the structure-I, II, III, respectively. Additionally, the structure-IV shows a satisfactory QF of 80.37 RIU^{-1}, FOM of 79.72 compared to the existed works. We also computed the overall performance parameter, i.e., CSF of 77.9 for the proposed structure. The achieved S performance of structure-IV is endorsed with the wavelength variation method. Also, with the field intensity performance, offering a very low value of R_{min} and high field intensity using transfer matric method. The high field intensity performance is endorsed with the FDTD solution. As the proposed SPR sensor is achieved a magnified value of S compared to the existing works due to the notable performance properties of the TIBr, therefore, it can be established a remarkable stage for biomedical and bio-sensing applications.

References

[1] M. Buscema, D. J. Groenendijk, S. I. Blanter, G. A. Steele, H. S. J. van der Zant, and A. Castellanos-Gomez, "Fast and broadband photoresponse of few-layer black phosphorus field-effect transistors," *Nano Lett.*, vol. 14, no. 6, pp. 3347–3352, Jun. 2014, doi: 10.1021/nl5008085.

[2] Y. Cai, G. Zhang, and Y.-W. Zhang, "Layer-dependent band alignment and work function of few-layer phosphorene," *Sci. Rep.*, vol. 4, no. 1, May 2015, Art. no. 6677.

[3] S.-Y. Cho *et al.*, "Superior chemical sensing performance of black phosphorus: Comparison with MoS_2 and graphene," *Adv. Mater.*, vol. 28, no. 32, pp. 7020–7028, Aug. 2016, doi: 10.1002/adma.201601167.

[4] B. K. Paul, K. Ahmed, D. Vigneswaran, F. Ahmed, S. Roy, and D. Abbott, "Quasi-photonic crystal fiber-based spectroscopic chemical sensor in the terahertz spectrum: Design and analysis," *IEEE Sensors J.*, vol. 18, no. 24, pp. 9948–9954, Dec. 2018, doi: 10.1109/JSEN.2018.2872892.

[5] H. Fu, S. Zhang, H. Chen, and J. Weng, "Graphene enhances the sensitivity of fiber-optic surface plasmon resonance biosensor," *IEEE Sensors J.*, vol. 15, no. 10, pp. 5478–5482, Oct. 2015.

[6] P. Englebienne, A. Van Hoonacker, and M. Verhas, "Surface plasmon resonance: Principles, methods and applications in biomedical sciences," *Spectroscopy*, vol. 17, nos. 2–3, pp. 255–273, 2003.

[7] S. W. Kowalczyk *et al.*, "Tuijt unrevealing single stranded DNA in solid state nanopore," *Nano Lett.*, vol. 10, no. 4, pp. 1414–1420, 2010.

[8] J. Homola, "Present and future of surface plasmon resonance biosensors," *Analy. Bioanaly. Chem.*, vol. 377, no. 3, pp. 39–528, Oct. 2003.

[9] S. K. Sharma, R. Jha, and B. D. Gupta, "Fiber-optic sensors based on surface plasmon resonance: A comprehensive review," *IEEE Sensors J.*, vol. 7, no. 8, pp. 1118–1128, Jun. 2007.

[10] V. Yesudasu, H. S. Pradhan, and R. J. Pandya, "Recent progress in surface plasmon resonance based sensors: A comprehensive review," *Heliyon*, vol. 7, no. 3, Mar. 2021, Art. no. e06321.

[11] L. E. Ronald, "Multiwavelength surface plasmon resonance sensor designs for chemical and biochemical detection," Ph.D. dissertation, Dept. Chem., Virginia Polytechnic Inst. State Univ., Toronto, ON, Canada, 2013.

[12] E. Klantsataya, A. François, H. Ebendorff-Heidepriem, P. Hoffmann, and T. Monro, "Surface plasmon scattering in exposed core optical fiber for enhanced resolution refractive index sensing," *Sensors*, vol. 15, no. 10, pp. 25090–25102, Sep. 2015, doi: 10.3390/s151025090.

[13] A. Verma, A. Prakash, and R. Tripathi, "Sensitivity enhancement of surface plasmon resonance biosensor using graphene and air gap," *Opt. Commun.*, vol. 357, pp. 106–112, Dec. 2015.

[14] J. Zhao, X. Zhang, C. R. Yonzon, A. J. Haes, and R. P. Van Duyne, "Localized surface plasmon resonance biosensors," *Nanomedicine*, vol. 1, no. 2, pp. 219–228, 2006, doi: 10.2217/17435889.1.2.219.

[15] K.-L. Lee, C.-W. Lee, W.-S. Wang, and P.-K. Wei, "Sensitive biosensor array using surface plasmon resonance on metallic nanoslits," *J. Biomed. Opt.*, vol. 12, no. 4, 2007, Art. no. 044023, doi: 10.1117/1.2772296.

[16] Y. K. Prajapati, A. Yadav, A. Verma, V. Singh, and J. P. Saini, "Effect of metamaterial layer on optical surface plasmon resonance sensor," *Optik-Int. J. Light Electron Opt.*, vol. 124, no. 18, pp. 3607–3610, Sep. 2013, doi: 10.1016/j.ijleo.2012.12.021.

[17] L. Wu, H. S. Chu, W. S. Koh, and E. P. Li, "Highly sensitive graphene biosensors based on surface plasmon resonance," *Opt. Exp.*, vol. 18, no. 14, pp. 14395–14400, 2010, doi: 10.1364/OE.18.014395.

[18] S. Pal *et al.*, "Sensitivity enhancement of metamaterial based surface plasmon resonance biosensor for near infrared," *Int. J. Opt. Appl.*, vol. 46, no. 1, pp. 131–143, 2016, doi: 10.5277/oa160112.

[19] J. B. Maurya, Y. K. Prajapati, V. Singh, and J. P. Saini, "Sensitivity enhancement of surface plasmon resonance sensor based on graphene–MoS_2 hybrid structure with TiO_2–SiO_2 composite layer," *Appl. Phys. A, Solids Surf.*, vol. 121, no. 2, pp. 525–533, Nov. 2015, doi: 10.1007/s00339-015-9442-3.

[20] S. Pal, A. Verma, Y. K. Prajapati, and J. P. Saini, "Influence of black phosphorous on performance of surface plasmon resonance biosensor," *Opt. Quantum Electron.*, vol. 49, no. 12, p. 403, Dec. 2017, doi: 10.1007/s11082-017-1237-7.

[21] N. Mao *et al.*, "Optical anisotropy of black phosphorus in the visible regime," *J. Amer. Chem. Soc.*, vol. 138, no. 1, pp. 300–305, 2016, doi: 10.1021/jacs.5b10685.

[22] V. Yesudasu, H. S. Pradhan, and R. J. Pandya, "SPR performance enhancement for DNA hybridization employing black phosphorus, silver, and silicon," *Appl. Opt.*, vol. 59, no. 24, pp. 7299–7307, Jan. 2020.

[23] S. Pal, A. Verma, J. P. Saini, and Y. K. Prajapati, "Sensitivity enhancement using silicon-black phosphorus-TDMC coated surface plasmon resonance biosensor," *IET Optoelectronics*, vol. 13, no. 4, pp. 196–201, Aug. 2019, doi: 10.1049/iet-opt.2018.5023.

[24] S. Pal, A. Verma, S. Raikwar, Y. K. Prajapati, and J. P. Saini, "Detection of DNA hybridization using graphene-coated black phosphorus surface plasmon resonance sensor," *Appl. Phys. A, Solids Surf.*, vol. 124, no. 5, pp. 1–11, May 2018, doi: 10.1007/s00339-018-1804-1.

[25] L. Wu *et al.*, "Sensitivity enhancement by using few-layer black phosphorus-graphene/TMDCs heterostructure in surface plasmon resonance biochemical sensor," *Sens. Actuators B, Chem.*, vol. 249, pp. 542–548, Oct. 2017.

[26] A. Srivastava, A. Verma, R. Das, and Y. K. Prajapati, "A theoretical approach to improve the performance of SPR biosensor using MXene and black phosphorus," *Optik*, vol. 203, Feb. 2020, Art. no. 163430, doi: 10.1016/j.ijleo.2019.163430.

[27] T. Srivastava and R. Jha, "Black phosphorus: A new platform for gaseous sensing based on surface plasmon resonance," *IEEE Photon. Technol. Lett.*, vol. 30, no. 4, pp. 319–322, Feb. 15, 2018.

[28] A. Lahav, M. Auslender, and I. Abdulhalim, "Sensitivity enhancement of guided-wave surface-plasmon resonance sensors," *Opt. Lett.*, vol. 33, no. 21, p. 2539, 2008.

[29] N. Mudgal, P. Yupapin, J. Ali, and G. Singh, "$BaTiO_3$-graphene-affinity layer–based surface plasmon resonance (SPR) biosensor for pseudomonas bacterial detection," *Plasmonics*, vol. 15, no. 5, pp. 1221–1229, Oct. 2020, doi: 10.1007/s11468-020-01146-2.

[30] L. Liu *et al.*, "Sensitivity enhancement of a graphene–barium titanate-based surface plasmon resonance biosensor with an Ag–Au bimetallic structure in the visible region," *J. Opt. Soc. Amer. B, Opt. Phys.*, vol. 36, no. 4, p. 1108, Apr. 2019, doi: 10.1364/JOSAB.36.001108.

[31] N. Mudgal, A. Saharia, A. Agarwal, and G. Singh, "ZnO and bi-metallic (Ag–Au) layers based surface plasmon resonance (SPR) biosensor with $BaTiO_3$ and graphene for biosensing applications," *IETE J. Res.*, vol. 4, pp. 1–8, Nov. 2020, doi: 10.1080/03772063.2020.1844074.

[32] D. J. Stukel and R. N. Euwema, "Energy-band structure of aluminum arsenide," *Phys. Rev.*, vol. 188, no. 3, pp. 1193–1196, Dec. 1969.

[33] H. T. Minden, "Some optical properties of aluminum arsenide," *Appl. Phys. Lett.*, vol. 17, no. 9, pp. 358–360, Nov. 1970.

[34] L. Guo, "Structural, energetic, and electronic properties of hydrogenated aluminum arsenide clusters," *J. Nanoparticle Res.*, vol. 13, no. 5, pp. 2029–2039, May 2011.

[35] A. Abbas, M. J. Linman, and Q. Cheng, "Sensitivity comparison of surface plasmon resonance and plasmon-waveguide resonance biosensors," *Sens. Actuators B, Chem.*, vol. 156, no. 1, pp. 169–175, Aug. 2011, doi: 10.1016/j.snb.2011.04.008.

[36] J. Whitaker, "Electrical properties of n-type aluminium arsenide," *Solid-State Electron.*, vol. 8, no. 8, pp. 649–652, Aug. 1965.

[37] K. Hitomi *et al.*, "Characterization of thallium bromide crystals for radiation detector applications," *J. Cry. Grow.*, vol. 225, nos. 2–4, pp. 129–133, May 2001, doi: 10.1016/S0022-0248.(01)00834-X.

[38] I. Pockrand, "Surface plasma oscillations at silver surfaces with thin transparent and absorbing coatings," *Surf. Sci.*, vol. 72, no. 3, pp. 577–588, Apr. 1978.

[39] Z. Lin, S. Chen, and C. Lin, "Sensitivity improvement of a surface plasmon resonance sensor based on two-dimensional materials hybrid structure in visible region: A theoretical study," *Sensors*, vol. 20, no. 9, p. 2445, Apr. 2020.

[40] L. Wu *et al.*, "Sensitivity improved SPR biosensor based on the MoS_2/graphene–aluminum hybrid structure," *J. Lightw. Technol.*, vol. 35, no. 1, pp. 82–87, Jan. 1, 2017, doi: 10.1109/JLT.2016.2624982.

[41] Z. Lin *et al.*, "Tuning and sensitivity enhancement of surface plasmon resonance biosensor with graphene covered Au-MoS 2-Au films," *IEEE Photon. J.*, vol. 8, no. 6, pp. 1–8, Dec. 2016, doi: 10.1109/JPHOT.2016.2631407.

[42] Y. Jia, Z. Li, H. Wang, M. Saeed, and H. Cai, "Sensitivity enhancement of a surface plasmon resonance sensor with platinum diselenide," *Sensors*, vol. 20, no. 1, p. 131, Dec. 2019.

[43] M. M. Rahman, M. M. Rana, M. S. Rahman, M. S. Anower, M. A. Mollah, and A. K. Paul, "Sensitivity enhancement of SPR biosensors employing heterostructure of $PtSe_2$ and 2D materials," *Opt. Mater.*, vol. 107, Sep. 2020, Art. no. 110123, doi: 10.1016/j.optmat.2020.110123.